This item is the archived peer-reviewed author-version of:
Three-dimensional multiphase modeling of the performance of an open-cathode PEM fuel cell with additional cooling channels

Reference:

Three-dimensional multiphase modeling of the performance of an open-cathode PEM fuel cell with additional cooling channels

Seyed Ali Atyabi[1] , Ebrahim Afshari[2*], Negar Shakarami[2]

1. VITO Sustainable Chemistry, Flemish Institute for Technological Research (VITO), Mol, Belgium

2. Department of Mechanical Engineering, Faculty of Engineering, University of Isfahan, Hezar Jerib Ave.,

Isfahan 81746- 73441, Iran

[*] Corresponding author: e.afshari@eng.ui.ac.ir

Abstract

Nowadays, there has been a growing interest in open-cathode polymer membrane fuel cells (PEMFCs) due to the absence of an external humidifier and the system's simplicity. This type of PEMFC uses air as both oxidant and coolant to maintain the required water content of the membrane for stable operation. In this work, the performance of a new strategy for improving cooling in open-cathode PEMFC is assessed and benchmarked against the conventional open-cathode PEMFC under similar operating conditions. With high air stoichiometry on the cathode side, air serves as both an oxidizer and a cooling medium, unlike conventional fuel cells, where cooling channels are installed separately. In order to compare two fuel cell cooling systems accurately, it is necessary to model electrochemical and thermal simulations simultaneously. A three-dimensional multiphase model is developed for the fuel cells and validated with experimental data. According to the simulation results, embedding separate cooling channels in PEMFC enhances cooling, consequently reducing the cell's temperature and stabilizing proton transfer across the membrane due to moderate water retention in the membrane. Distinct behaviors were observed in the three zones of the polarization curve for both fuel cells. While the conventional open-cathode PEMFC revealed lower losses in the polarisation curve's activation and concentration loss zones, the case with additional cooling channels exhibited lesser losses in the ohmic zone caused by improved cooling. Although the difference in maximum output power at 0.65 V voltage reached 6.3 W for the case with additional cooling channels, the parasitic load due to the pressure drop in this fuel cell is 0.34 W, higher than the conventional fuel cell obtained at 0.03 W.

Keywords: PEMFC, open-cathode, high stoichiometry, cooling channels, water content, air cooling

Introduction

The negative impacts of fossil fuel consumption on the environment are irreversible, hence, the growing interest in cleaner fuels and accompanying technologies. Hydrogen is a cleaner

fuel that produces water when combusted and generates electricity using fuel cells capable of supplying energy for stationary and portable applications. Polymer electrolyte membrane fuel cells (PEMFCs), among other fuel cell types, are already being adopted in the transportation sector because of their technological advantages such as quick start-up and shut down, fast dynamic response, low noise, low operating temperature, high efficiency, and safety [1]. Toyota, BMW, and Honda are leading brands in the manufacture of fuel-cell vehicles, with Toyota releasing its first commercial car in 2015 [2,3]. PEMFCs are also growing in popularity in the aerospace industry, and numerous projects are looking to use them in commercial passenger aircraft. In applications such as drones, lithium-ion batteries are not potentially beneficial if flight durability and continuous environmental monitoring are required. Due to their low energy density, they cannot supply sufficient power for long flight durations [4]. On the contrary, PEMFCs can be used for longer flight durations because of their remarkable features, such as high energy density and speedy refueling time.

It is common for commercial PEMFC systems to use one cooling fluid (liquid water or air). To circulate cooling inside the stack, liquid fluid must be used as a cooling fluid. Liquid flow through channels created inside bipolar plates. Consequently, the liquid absorbs the heat produced by the fuel cell. Radiators cool the warm water coming out of the stack and return it to the stack. In this method, a lot of equipment (radiator, pump, water tank, etc.) is needed, which increases the volume, weight, costs, and parasitic power of the system, and therefore water cooling is generally necessary for High-power PEMFCs. In order to overcome these problems, air can be used as a cooling fluid, a channel is created parallel to the fan, which allows ambient air to enter the cell and cool it. In addition, instead of air flowing inside the cooling channels, more air can enter the cathode channels (increasing the cathode stoichiometry). Most of the air is removed by absorbing the generated heat, while a small amount is used as an oxidizer inside the cell.

PEMFCs function on hydrogen as fuel with pure oxygen or air as oxidant. Although pure oxygen has been shown to achieve high performance and efficiency, it imposes a cost penalty due to pure oxygen production and storage and reduces convective heat removal by the outlet moisture [5]. Accordingly, air is commonly used and can be delivered to the fuel cell as an oxidizer and coolant; in the presence of other subsystems such as cooler and humidifier in an arrangement referred to as closed cathode, or directly without the use of cooling or humidification systems in a method called the open cathode. Open-cathode PEMFCs operate by the transport of ambient air to the system, wherein the cathode inlet and outlet channels are exposed to the surrounding. This type of configuration is classified into forced and natural

convection open-cathode PEMFCs [6]. In natural convection, ambient air flows into the open-cathode channel in the absence of a fan, due to temperature and concentration gradient, whereas in forced convection, the fan is used to propel air into the cathode channel [7]. The latter has been disclosed to demonstrate better performance than the former, according to the study completed by Sasmito et al. [6]. Natural convection open-cathode PEMFC was reported to show good performance for a few numbers of cells in a fuel cell stack (up to 12), above which forced convection open-cathode PEMFC was observed to maintain higher cell performance. Open-cathode PEMFC is attracting a lot of research interest partly due to its ability to generate substantial power density with a simple design that air can act as both a cooling and oxidant supply. However, this arrangement usually has relatively low performance compared to a pressurized fuel cell due to the low oxygen concentration, consequently low reaction rates [5]. Furthermore, maintaining membrane hydration and successful cooling of PEMFC, especially in high current density, is difficult due to the lack of an external humidifier [8]. Open-cathode PEMFC can also lead to unequal temperature distribution and create hotspots that affect membrane protonic conductivity. Air flow in separate cooling channels and increased air flow rate in the cathode channels affect the electrochemical performance of cell. PEMFC electrochemical performance is affected by the quality of its cooling in two ways: by changing its temperature and by changing its rate of electrochemical reactions (activation overvoltage). Likewise, it occurs in the opposite direction. The electrochemical performance of PEMFC greatly impacts its temperature, and thus its cooling quality. For that reason, it is imperative that a numerical, three-dimensional and two-phase model of PEMFC, which includes electrochemical sections and cooling channels, is analyzed together with the electrochemical system, and that they are compared so that the best cooling system can be chosen.

López-Sabirón et al. [9] designed and developed a forced convection open-cathode for a 2kW PEMFC. Although the airflow rate needed to keep the cell temperature at the desired level by removing excess heat was supplied, a non-uniform temperature distribution was observed along with the stack. Though, the behavior was attributed to the fan assembly and configuration. Research is currently directed towards improving and developing cathode designs and strategies to improve membrane water retention and reduce temperature variation in fuel cell systems.

Liu et al. [10] presented a two-dimensional model of a polymer membrane fuel cell. In their work, the electrochemical reactions in both anode and cathode catalyst layers, the diffusion of reactants in the gas diffusion layers and the gas flow in the channels have been modeled. The

results show that the concentration gradient mainly occurs on the cathode side of the fuel cell. Also, the concentration of hydrogen and oxygen decreased along the channel flow direction. Three types of PEMFCs, including parallel flow channels, pin-type channels, and metal foam are compared by Afshari et al. [11]. According to their results, pin-type channels or foam increase the average current density. In addition, metal foam provides a more uniform distribution of current density than the other two models. Abdollahzadeh et al. [12] developed a two-dimensional model to study the performance of PEMFCs with a different configurations of gas channels. A multi-phase mixed model has been used to simulate the two-phase flow in this study. Various geometrical and operational factors were also investigated parametrically. Their results show that this model can accurately predict the performance of fuel cells based on different parameters. An electrochemical model for PEMFCs is presented by Rahgoshay et al. [13] .They compared two types of serpentine and parallel cooling flow fields with a model without cooling flow fields. In their study, it was shown that changing the heat transfer rate affects the fuel cell's performance. According to the effective physical parameters, the parallel model has a better performance than the serpentine model. According to Pan et al. [14], a polymer membrane fuel cell can be designed based on different flow fields. The results indicate that different flow field models are affected by temperature and voltage. Cai et al. [15], proposed an optimal three-dimensional cathodic current field exists with three main channels, sub-channels, and transition zones. The performance of these 3D models has been compared with straight channels. The results show that the fuel cell with a three-dimensional cathode current field performs much better than the PEMFC with conventional straight channels.

Karst et al. [16] proposed a new method to maintain the hydration of the membrane by changing the opening ratio of the inlet channel. Their results show that the removed water from the cathode side increases with low opening ratios. They also found that the maximum back diffusion (about 33%) of produced water occurred at a current density of 150 mA cm^{-2} with a cover ratio of 5%. Matian et al. [17] investigated three different flow field designs for open-cathode PEMFC cooling in a numerical and experimental study. They showed that using wider channels improves forced convection, enhances heat transfer, and decreases parasitic load. Qiu et al. [18] developed a three-dimensional air-cooled PEMFC to optimize the geometrical features of cathode channels. They found that a rib-channel ratio within a range of 3.0 is suitable to enhance the PEMFC's performance. Zhao et al. [19] conducted an experimental study using heat spreaders to enhance 10-cell air-cooled stack thermal management. Their results indicated that using this method enhances the uniformity of temperature in the stack,

and the maximum temperature gradient between the cell and within the active area at 0.64 A cm^{-2} was reported to be 5.3 and 1.5°C, respectively. Kang et al. [20] proposed the application of metal foam on the cathode side to improve performance. Their findings revealed that employing metal foam enhances the evaporation of produced water at the cathode side, and a 25% increase in performance could be obtained. Sagar et al. [21] developed a generic numerical model for an air-cooled open-cathode PEMFC and compared simulation results with liquid-cooled PEMFC. They reported higher performance for the liquid-cooled PEMFC than the open-cathode PEMFC due to poor thermal, and water management observed in the open-cathode fuel cell. However, it was concluded that an open-cathode PEMFC could perform well even at high temperatures and high relative humidity with a proper strategy.

To address the issue of uneven temperature distribution and consequent membrane failure observed in open-cathode PEMFC, Huang et al. [22] suggested a novel cooling method for a 10-cell open-cathode PEMFC stack. They found that the inclination angle influences the thermal management of PEMFCs at a small flow rate. Similarly, Lee et al. [23] simulated two different flow fields (metal-foam-based and smaller cathode inlet) to prevent membrane dehydration and unstable operating. They found a more uniform distribution of reactant flow and temperature in a metal-foam-based design. Furthermore, their results show that their modification on the cathode inlet area has a negligible effect on the water content and hydration of the membrane. More recently, Lee et al. [24] designed and modeled an innovative cathode plate with separate channels for cooling air and reactant air. Significant improvements in membrane water retention and airflow distributions were reported for the fuel cell. However, this performance may likely have been downplayed or exaggerated due to the single-phase model adopted. Single-phase models are known to overpredict the performance of a fuel cell due to failure to account for the existence of liquid water in flow channels [25,26].

Compared to previous studies, there have been relatively few studies of the simultaneous electrochemical-thermal investigation of PEMFCs with increasing air stoichiometry, which also function as cooling devices. This work presents a three-dimensional and multi-phase electrochemical-thermal model of a single PEMFC, and the performance under two cooling methods has been investigated in an open-cathode PEMFC. In the first method, a newly designed open-cathode PEMFC with separate cooling and gas channels has been considered to manage membrane water content within an appropriate range, enhance ionic conductivity, and achieve high uniformity in temperature distribution and current density. In the second method, the effect of excess air on the electrochemical performance and cooling of the battery has been

seen simultaneously. The performance of PEMFC with two different methods is compared under the same operating conditions and geometric dimensions.

Model development

This work employed an advanced Computational Fluid Dynamic (CFD) numerical model to model a single PEM cell for two forced open-cathode PEMFC configurations. A single PEMFC was considered due to the computational demand of modeling the whole fuel cell stack. CFD is a reliable method to predict fluid flow's motion and heat transfer whereby the model is validated using experimental data obtained from the literature and can be applied to fuel cells to estimate PEMFC behavior at a low cost. However, because of the complex phenomena occurring in PEMFC, this approach has some drawbacks that could affect the accurate modeling of the cell. These limitations include numerical solution errors due to a wide range of sizes from centimeters to micrometers, inaccurate generalization predictions of a cell to stack outcomes, and vague estimates of PEMFC performance.

This work comprises two three-dimensional models of open-cathode PEMFC with (case A) and without (case B) cooling channels, with the PEMFC possessing an active area of 70 cm^2 and consisting of gas diffusion layer (GDL), Micro Porous Layer (MPL), catalyst layer (CL), bipolar (BPP), and membrane (Fig. 1). Both fuel cells have 28 cathode gas flow channels and 20 anode gas flow channels each, in a cross-flow flow field design, with case B featuring an additional cooling plate containing 14 parallel cooling channels [27].
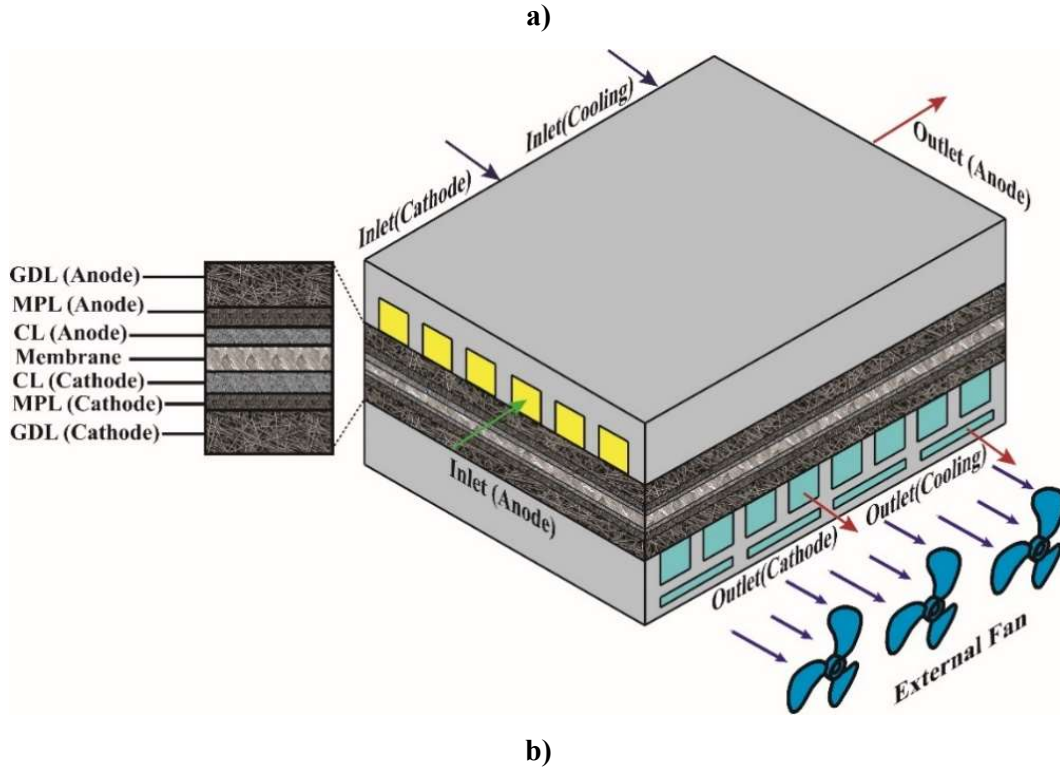
a)

b)
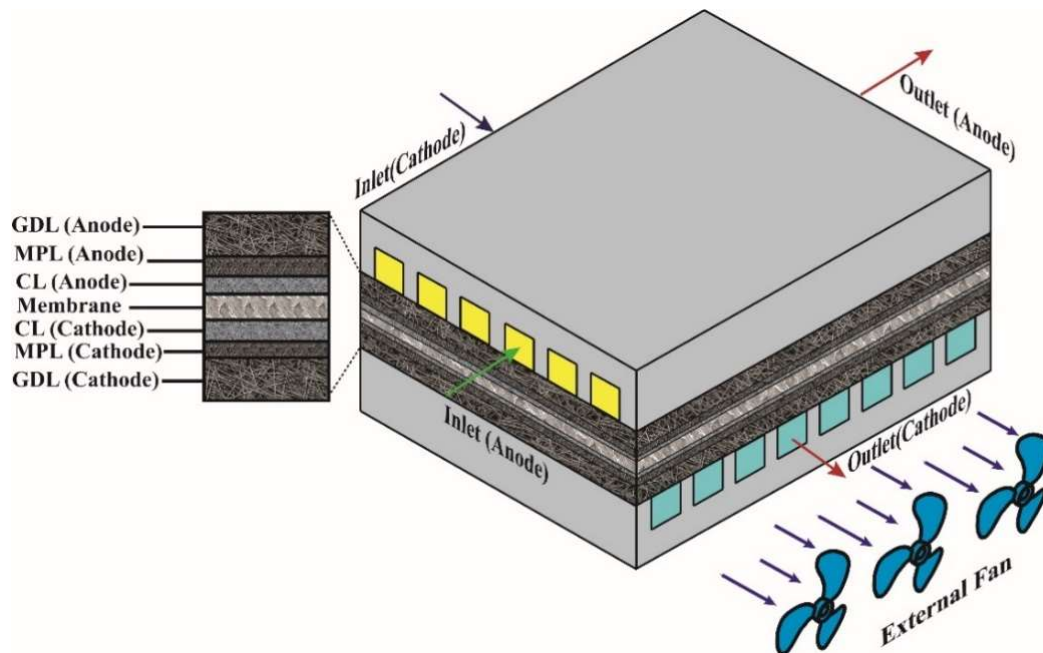
Fig. 1. Schematic view of cross-flow PEMFC design a) without and b) with cooling channels and main components

Assumptions

To simplify the complexity of the model, assumptions are applied as follows:

(1) Mixtures of reactant gases are considered ideal gas (due to the low-pressure range) at constant pressure.

(2) Since the polymer membrane fuel cell starts in a few seconds, like many studies, this study examines the steady state performance of the cell.

(3) Fluid flow streams are incompressible (M <0.3) and assumed to be in the laminar flow regime (Re <2300)

(4) In all porous regions, including GDL, CL, MPL, and membrane, the porosity and permeability are assumed constant [28].

(5) The effect of gravity is not considered in the simulation [28].

(6) The isothermal condition is also used in some references for walls; However, due to the series of cells and the construction of the stack, the adiabatic condition is more suitable for the outer walls.

(7) Airflow rate can be provided by the fan from the fan-system characteristic curve described in Ref [26]. Therefore, the fan is not modeled, and varying air flow rates were applied instead.

Governing equations

The governing equations, including conservation of mass, momentum, energy, and species, have been modified based on the assumptions above. In addition to fluid flow equations, electrochemical equations are used to investigate the behavior of the PEMFC. Governing equations and the source terms for each zone are presented in Table 1, while the constitutive equations are given in Table 2.

Table 1. Governing equations for PEMFC with source/sink terms

Equations	Expression	
Continuity	$\nabla \cdot (\rho \vec{u}) = 0$	(1)
Momentum	$S_u = -\dfrac{\mu}{K_p}\vec{u}$ **(In porous media zone)** $\left(\dfrac{1}{\varepsilon^2}\right)\nabla \cdot (\rho \vec{u}\vec{u}) = -\nabla P + \nabla \tau + S_u$	(2)
Species	$\nabla \cdot (\gamma_i \rho m_i \vec{u}) = \nabla \cdot \left[\rho^g D_i^{g,eff}\nabla(m_i^g)\right] + \nabla \cdot \left[(m_i^g - m_i^l)\vec{j}^l\right] + S_i$ **(for water in CLs and membrane),** $S_i = \left[-\nabla \cdot \left(\dfrac{n_d}{F}\vec{I}\right) + \dfrac{s_i j}{nF}\right]M_i$	(3)
	$S_i = \left[\dfrac{s_i j}{nF}\right]M_i$ **(other species in CLs)**	
	$\nabla \cdot \left[\left(\dfrac{\rho^{mem}}{EW}\right)D_W^{mem}\nabla\lambda\right]M_W - \nabla \cdot \left[n_d\left(\dfrac{I}{F}\right)\right]M_W + \nabla \cdot \left[\left(\dfrac{\kappa^{mem}}{\upsilon^l}\right)\nabla P^l\right] = 0$	(4)
	$\dfrac{\partial(\varepsilon \rho_l s)}{\partial t} + \nabla \cdot (\rho_l \vec{v}_l s) = r_w$; $\vec{v}_l = \dfrac{k_p s^3}{\mu_l}\dfrac{dP_c}{ds}$	
Water formation	$r_w = \begin{cases} (1-s)c_r \dfrac{p_{wv} - p_{sat}}{RT}M_{H_2O} & \text{if } (p_{wv} > p_{sat}) \\ sc_r \dfrac{p_{wv} - p_{sat}}{RT}M_{H_2O} & \text{if } (p_{wv} < p_{sat}) \end{cases}$	(5)
Energy	$S_T = j\left(\eta - T\dfrac{dU_0}{dT}\right) + \dfrac{I^2}{k^{eff}}$ $S_T = \dfrac{I_e^2}{k^{eff}}$ $\nabla \cdot (\rho \vec{u} C_p^g T) = \nabla \cdot (k^{eff}\nabla T) + S_T$ $S_T = h_{fg}\nabla \cdot \left(\dfrac{K}{\nu}\lambda^l \lambda^g \nabla P_c + \lambda^l \rho \vec{u}\right)$ **(two-phase region),**	(6)
Charge	**Proton transport:** $\nabla \cdot (\sigma^{mem}\nabla\varphi_e) + S_\varphi = 0$; **Electron transport:** $\nabla \cdot (\sigma^{eff}\nabla\varphi_s) - S_\varphi = 0$	(7)
	$S_\varphi = j$	(8)
Electrochemical reactions	$\sum_k s_i M_i^z = ne^-$, where $\begin{cases} M_i = \text{chemical formula of species i} \\ s_i = \text{stoichiometric coefficient} \\ n = \text{number of electrons transfered} \end{cases}$	(9)
	Anode: $H_2 - 2H^+ = 2e^-$; Cathode: $2H_2O - O_2 - 4H^+ = 4e^-$	
	In anode CL:	
Current density (Butler-volmer)	$j = (1-s)^{1.5}a_r j_{0,a}^{ref}\left(\dfrac{C_{H_2}}{C_{H_2,ref}}\right)^{\frac{1}{2}}\exp\left[-\dfrac{E_a}{R}\left(\dfrac{1}{T} - \dfrac{1}{353.2}\right)\right]\left(\exp\left(\dfrac{\alpha_a + \alpha_c}{RT}\right)F\eta\right)$	(10)
	In cathode CL:	(11)

$$j = -a_r j_{0,c}^{ref} \left(\frac{C_{O_2}}{C_{O_2,ref}} \right)^{\frac{3}{4}} \exp\left[-\frac{E_a}{R}\left(\frac{1}{T} - \frac{1}{353.2} \right) \right] \left(\exp\left(-\frac{\alpha_c}{RT} \right) F\eta \right)$$

Overpotential	**anode CL:** $\eta = \varphi_s - \varphi_e$; **cathode CL:** $\eta = \varphi_s - \varphi_e - E_0$ $E_0 = 1.229 - 0.9 \times 10^{-4}(T - 298.2)$ **(12)**

Table 2. Constitutive equations

Equation	Expression	
Permeability of GDL	$K_p = \dfrac{d_p^2}{150} \dfrac{\varepsilon^3}{(1-\varepsilon)^2}$	**(13)**
Diffusivity coefficient	$D_i^{eff} = \varepsilon^{0.5}(1-s)^{r_s} D_i^0 \left(\dfrac{p_0}{p} \right)\left(\dfrac{T}{T_0} \right)^{1.5}$	**(14)**
Protonic conductivity	$\sigma^{mem} = (0.5139\lambda - 0.326)\exp\left[1268\left(\dfrac{1}{303} - \dfrac{1}{T} \right) \right]$	**(15)**
Electrical conductivity	$\sigma^{eff} = \dfrac{\sigma_{comp} \cdot h_{initial}}{h_{comp}}$	**(16)**
Contact resistance	$R_{GDL/BP} = 2.2163 + \dfrac{3.5306 A_{contact}}{P_{Assembly} A_{Assembly}}$	**(17)**
Capillary pressure	$P_c = P^g - P^l = \sigma_{surf} \cos\theta_c \left(\dfrac{\varepsilon}{K_p} \right)^{\frac{1}{2}} J(s)$	**(18)**
Leverett function	$J(s) = \begin{cases} 1.417(1-s) - 2.12(1-s)^2 + 1.263(1-s)^3 & \text{if } \theta_c < 90 \\ 1.417s - 2.12s^2 + 1.263s^3 & \text{if } \theta_c > 90 \end{cases}$	**(19)**
Water activity	$a = \dfrac{p_{wv}}{p_{sat}} + 2s$	**(20)**
Electroosmotic drag coefficient	$n_d = \dfrac{2.5\lambda}{22}$	**(21)**
Membrane water content	$\lambda = \begin{cases} 0.043 - 17.81a - 39.85a^2 + 36a^3 & \text{for } 0 < a \leq 1 \\ 22 & \text{other} \end{cases}$	**(22)**
Membrane water diffusivity	$D_w = f(\lambda)\exp\left[2416\left(\dfrac{1}{303} - \dfrac{1}{T_{cell}} \right) \right]$ $f(\lambda) = \begin{cases} 3.1\times10^{-7}\lambda(\exp(0.28\lambda) - 1)\exp(\dfrac{-2346}{T_{cell}}) & 0 \leq \lambda \leq 3 \\ 4.17\times10^{-8}\lambda(161\exp(-\lambda) + 1)\exp(\dfrac{-2346}{T_{cell}}) & \lambda > 3 \end{cases}$	**(23)**
Saturation pressure	$\log_{10}(p_{sat}/101325) = -2.1794 + 0.02953\Delta T - 9.1837\times10^{-5}\Delta T^2 + 1.4454\times10^{-7}\Delta T^3$ $\Delta T = T - 273.2$	**(24)**

Boundary conditions and numerical process

At the inlet, velocity inlet is selected for both the gas and cooling channels, while pressure outlet boundary is set at the outlet of the channels (back pressure of anode and cathode side is equal to 1 atm). The following equation is used to estimate the anode and cathode velocities of a PEMFC:

$$u_{in,a} = \frac{\zeta_a I A_{mea}}{2 C_{H_2} F A_{a,channel}} \tag{25}$$

$$u_{in,c} = \frac{(U_0 - T \dfrac{d U_0}{d T} - V_{cell}) I A_{mea}}{\rho C_p A_{inlet} (T_{out} - T_{in})} \tag{26}$$

At the inlet, the velocity value for anode, cathode and cooling channels are 3, 2-5 and 2-5 m/s, respectively. Mass fraction of H_2, O_2 and H_2O at the anode and cathode side are 0.99, 0.2 and 0.01, respectively. Relative humidity of anode and cathode is considered 30% and the temperature of the cooling channel is 300 K. Channels thermally coupled to the fuel cell domain were assigned the no-slip boundary condition, while the side walls were set to zero heat flux. Both anode and cathode gas channels have an interface with GDL without boundary conditions. On the cathode side, the boundary condition for the electric current collector is equal to the operating voltage.

Finite volume method is used to solve the conservation equations. In the first-order upwind method, electrical charge and membrane water content are discretized, whereas, in the second-order upwind method, the momentum, species, and energy equations are discretized. The pressure-based solver is applied due to the incompressibility and laminar flow of the gases. In this approach, the momentum equations are solved to obtain velocity values throughout the entire numerical domain. The momentum and continuity equations are modified to give the pressure correction equation, and the SIMPLE approach solver, which runs by guessing pressure, is used to define the pressure-velocity relation. The convergence criteria for solutions are based on residual values for the mass conservation is 1×10^{-4} and for energy conservation is 1×10^{-6}. The bi-gradient approach has been used to accelerate the convergency, where the computations are transferred from the fine to the large grid area or vice versa using the F-cycle multi-grid method. Under-relax factors for momentum, pressure, and mass species are adjusted to 0.3, 0.7, and 0.98, respectively. PEMFC simulations are implemented in Ansys19.2 software, using core-i7 processors (Intel @ 2.27 GHz and 16 GB DDR 3 RAM), with each case taking around 30 hours to complete. Table 3 shows the required parameters used for the PEMFC modeling. The numerical solution flowchart is shown in Fig. 2.
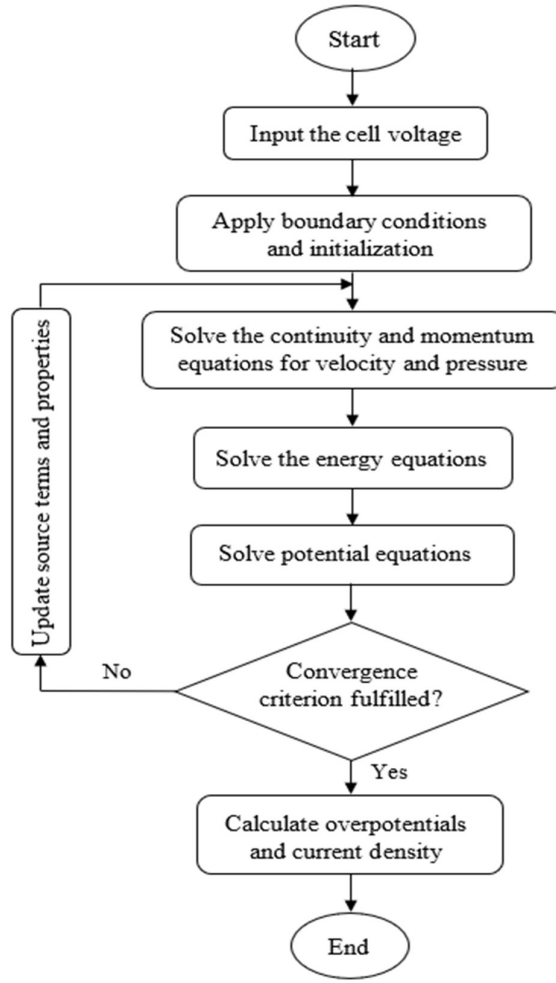
Fig. 2. Numerical solution flowchart

Table 3. Geometrical, electrochemical, thermal features of PEMFC model

Parameter	Values
Thickness of BPP (anode, cathode)/GDL/CL/mem, $((t_{BPP,a}/t_{BPP,c})/t_{GDL}/t_{MPL}/t_{CL}/t_{mm})$	(2, 2.5)/0.3/0.03/0.03/0.051 mm
Height of cell/gas channel/ cooling channel ($H_{cell}/H_{ch}/H_{cool}$)	6.271/1/1 mm
Width of cell/gas channel/cooling channel/rib, ($W_{cell}/W_{ch}/W_{cool}/W_{rib}$)	71.5/2/5.5/1.5 mm
Length of cell/gas channel (anode, cathode)/cooling channel, ($L_{cell}/L_{ch,a}$, $L_{ch,c}/L_{cool}$)	141.5/ (141.5, 71.5)/71.5 mm
Reference current density of anode/cathode, ($i_{0,a}^{ref}/i_{0,c}^{ref}$)	6×10^4/0.3 A m^{-2}
Average current density of cell, (I_{avg})	1×10^4 A m^{-2}
Reference H$_2$/O$_2$ molar concentration, ($C_{H_2,ref}/C_{O_2,ref}$)	kmol m^{-3} 0.04/0.04
Concentration exponent for anode/cathode, (γ_a/γ_c)	0.5/0.75
anode/cathode, (α_a/α_c) of Exchange coefficient	1/1
Reference diffusivity of H$_2$/ H$_2$O/N$_2$/O$_2$, ($D_{H_2}^0/D_{H_2O}^0/D_{N_2}^0/D_{O_2}^0$)	s$^-$ 1.1×10^{-4}/7.35×10^{-5}/3×10^{-5} /3.2×10^{-4} m$^2_1$
Thermal conductivity of H$_2$/ H$_2$O/N$_2$/O$_2$, ($k_{H_2}/k_{H_2O}/k_{N_2}/k_{O_2}$)	m^{-1}K^{-1} 0.2040/0.0237/0.0293/0.029 W
Specific heat capacity of H$_2$/O$_2$ /H$_2$O, ($C_{p,H_2}/C_{p,O_2}/C_{p,H_2O}$)	kg^{-1}K^{-1} 14283/919.3/2014 J

Viscosity of H_2/O_2/H_2O, (μ_{H_2}/μ_{O_2}/μ_{H_2O})	8.4×10^{-6}/1.9×10^{-5}/1.3×10^{-5} kg m^{-1}s^{-1}
Saturation exponent for blockage, (r_s)	2.5
Pore blockage for transfer current, (r)	2.5
Water condensation rate, (c_r)	100 s^{-1}
Contact resistance between GDL and BPP, ($1/\sigma$)	2.6×10^{-7} S^{-1} m
Density of BPP/GDL/CL/mem, (ρ_{BPP}/ρ_{GDL}/ρ_{CL}/ρ_{mem})	2719/2719/2719/2000 kg.m^{-3}
Specific heat capacity of BPP/GDL/CL/mem, ($C_{p,BPP}$/$C_{p,GDL}$/$C_{p,CL}$/$C_{p,mem}$)	kg^{-1}K^{-1} 871/871/871/2000 J
Thermal conductivity of BPP/GDL/CL/mem, (k_{BPP}/k_{GDL}/k_{CL}/k_{mem})	m^{-1}K^{-1} 16.2/1.2/1.5/0.95 W
Electronic conductivity in BPP/GDL/CL/mem, (σ_{BPP}/σ_{GDL}/σ_{CL}/σ_{mem})	2×10^4/15750/1000/1×10^{-16} S m^{-1}
Porosity of GDL/CL/mem, (ε_{GDL}/ε_{CL}/ε_{mem})	0.6/0.4/0.4
Permeability of GDL/CL/mem, (K_{GDL}/K_{CL}/K_{mem})	m^{-2} 1×10^{-12}/1×10^{-13}/1×10^{-30}
Contact angles of GDL/CL, (θ_{GDL}/θ_{CL})	92°/92°
Surface to volume ratio, (s_r)	2.0×10^5 m^{-1}
Equivalent weight of mem, (M_m)	kmol^{-1} 1100 kg
Operating pressure, (P)	1 atm
Operating temperature, (T)	333 K

Mesh study

To reduce shear errors, the mesh resolution should be as fine as possible. The source of the error in numerical simulation is in the process of discretization. The independence mesh study for the numerical model is performed by using four different types of meshes: coarser, coarse, fine, and finer with the number of elements 1309960, 1436000, 1524901 and 1746859, respectively. The average current density at 0.6 V is adopted to compare the different meshes. Current density increases linearly as the mesh density increases from coarser to coarse. The mesh study curve is depicted in Fig. 3. Since the results for the two mesh types (fine and finer) are fairly close, the fine mesh is chosen as the mesh to use for numerical modeling. By choosing fine mesh with 1524901 elements, independency for solution is achieved, as shown in the experimental results [29].
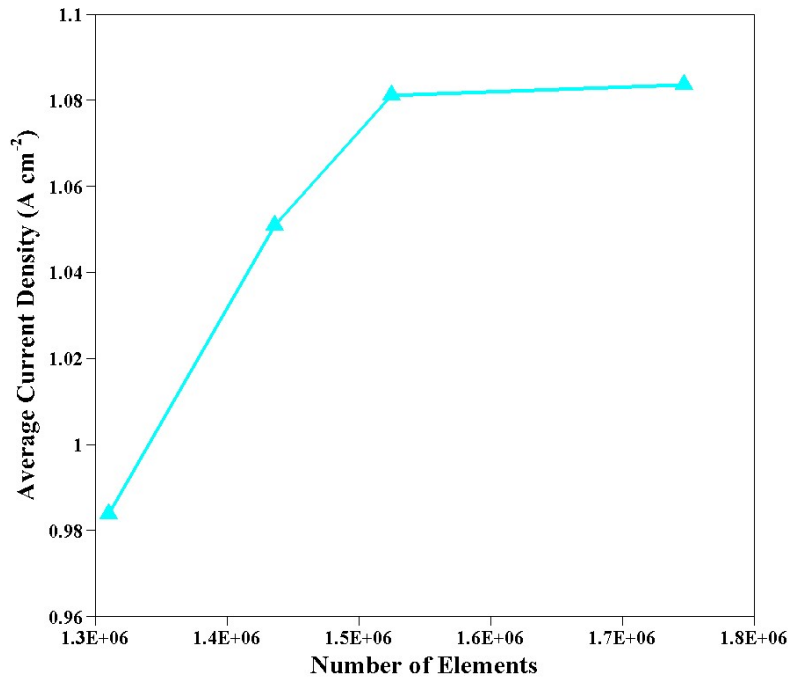
Fig. 3. The dependency of the average current density on the number of the computational cell

Validation

Model validation was carried out by comparing the resulting polarisation curve for the open-cathode PEMFC without cooling with experimental data obtained from literature, as shown in Fig. 4. The experimental polarization curve and numerical model provide comparable results. In the first logarithmic section of the curve, activation losses are significant, and an acceptable difference is seen between the model and experiment. This difference is because the theoretical voltage used in the modeling relationships differs from the observed voltage. In the second part, where ohmic losses dominate, there is a minimal difference, and the errors are around 3-4 percent. Therefore, numerical results and experimental data can be concluded to have a good agreement, and the electrochemical model is adopted to analyse the case presented in this work.
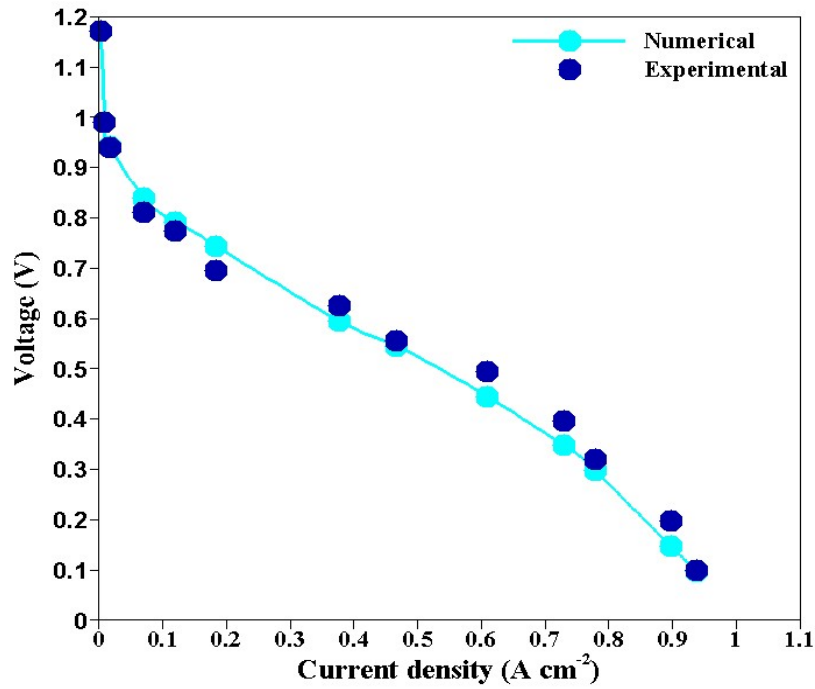
Fig. 4. Comparison of the polarization curve of the present numerical results with the reference data [29]

Results and discussion

The open-cathode PEMFC (without cooling channels) model has been validated with experimental data obtained from literature. Therefore, extending the validated numerical model to the case with cooling channels under similar conditions is reasonable.

3.1. Fuel cell temperature

The performance of fuel cells is hampered by two problems: membrane dryness and water flooding. Dehydrated membrane may occur due to insufficient cooling performance, thereby reducing water content and cell performance, especially in the ohmic zone. On the other hand, excessive transfer of produced water to cells could lead to water flooding and blockage of the GDL's pores and, consequently, a reduction in air transfer to the CL. For a stable and efficient operation of a fuel cell, in addition to maintaining the membrane water content to prevent water flooding, the produced water on the cathode side must be removed from the cell [5]. In this section, the cell temperatures for both cases have been compared under varying air velocities. Increasing the air velocity is expected to impact the maximum temperature of fuel cell components such as GDL, membrane and catalyst layer, which can influence the cell performance due to the direct relationship between high temperature and water in the fuel cell. Hence, Fig. 5 depicts the temperature distribution at the CL-membrane interface on the anode

side for both cases at different inlet velocities (2-5 m/s). In reality, higher air velocity is achieved by increased airflow rate resulting from the improved power rating of the fan [6]. As can be seen in Fig. 5, the temperature distribution varies slightly across the different velocities, with the maximum temperature gradient for the baseline case reaching 4.6K, corresponding closely to the results of Ref. [18,30]. In the case with cooling channels, the maximum temperature observed within the fuel cell was relatively lower at 328.2K and increased linearly from the inlet to the outlet region along with the interface. The contour temperature distribution for both cases appears to be similar across the various velocities, indicating that the heat accumulation at the anode outlet will always be higher irrespective of the air velocity. Ultimately, only a slight reduction in temperature (6.5 K) is observed in case A compared to the baseline case B.

In addition to limitations in temperature, it may also not be uniform inside PEMFCs. Various cell locations experience different rates of electrochemical reactions due to nonuniformity of temperature. As a result, hot spots occur at certain locations of the cell, decreasing the durability of the fuel cell. As a consequence, it is very important to know how the temperature distribution inside a fuel cell is distributed. Standard deviation (SD) can be used to determine temperature uniformity. When this index is smaller, the temperature distribution is more uniform. In a fuel cell without cooling channels, SD is 2.8, 2.6, 2.5 and 2.3 for cathode velocities of 2, 3, 4 and 5 m/s. By increasing airflow rate, this index decreased, resulting in a more uniform temperature at the CL-Mem interface. In addition, when comparing two cases (A and B), it becomes clear that the temperature uniformity is nearly the same, and the difference in this index decreases as the airflow rate increases.
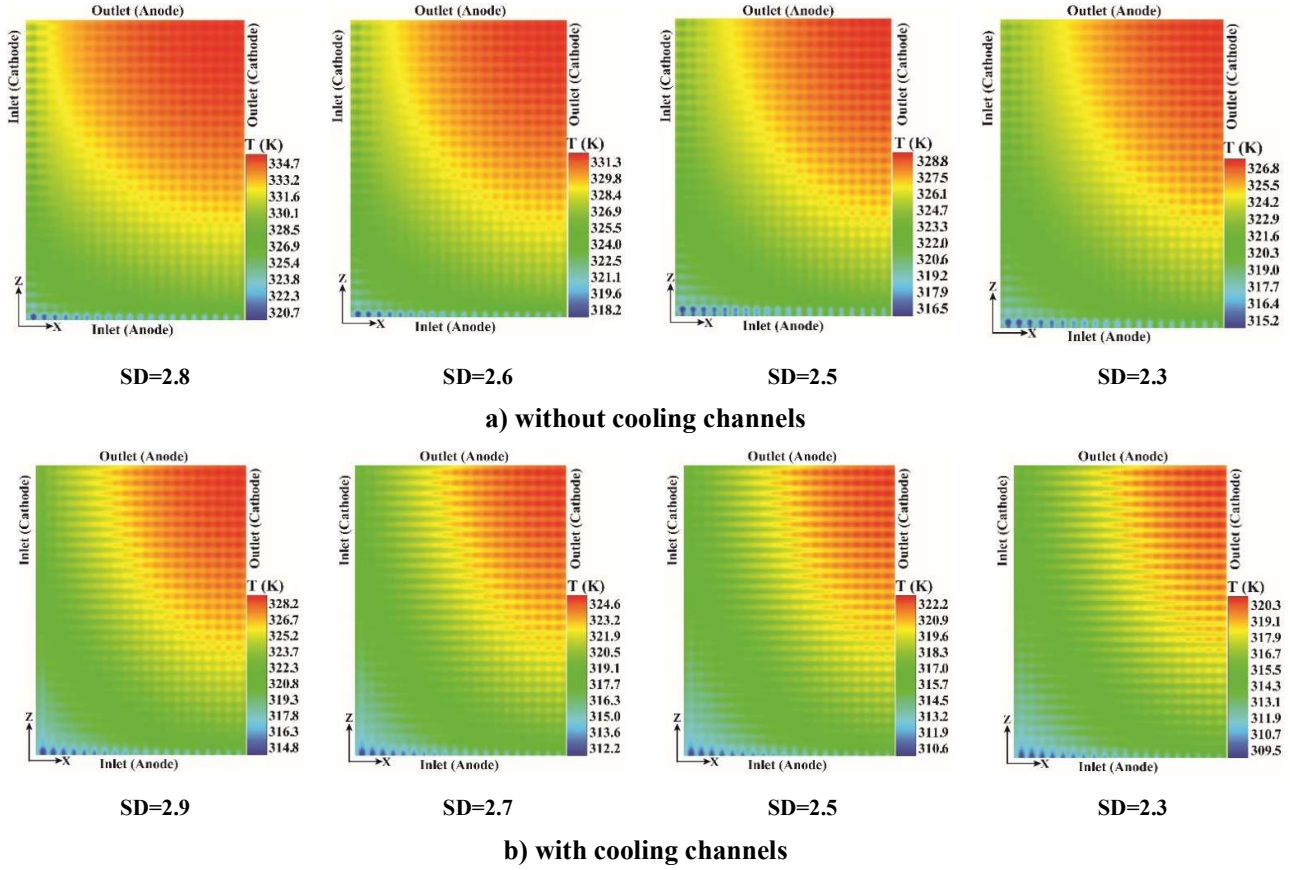
V=2 m/s   **V=3 m/s**   **V=4 m/s**   **V=5 m/s**

SD=2.8   SD=2.6   SD=2.5   SD=2.3

a) without cooling channels

SD=2.9   SD=2.7   SD=2.5   SD=2.3

b) with cooling channels

Fig .5 .Comparison of temperature at CL-Mem interface (where SD – Standard deviation)

3.2.   Water and oxygen distribution

Protonic conductivity of the fuel cell membrane is diminished in the absence of water content, thus affecting fuel cell performance [31]. Water content contours across the cathode CL-MEM interface for cases A and B are shown in Fig. 6. Water content is relatively high near the zone of the cathode inlet and decreases near the cathode outlet as a result of the increase in local temperature from cathode inlet to outlet, as discussed in Section 3.1. The water content and concentration across the GDL and CL-MEM interface have been compared between the open-cathode PEMFC with cooling channels and the baseline case. In Fig. 6a and b, the water content reduces along with the GDL-CL interface from the cathode inlet to the outlet and increases with rising air velocities due to reduced air capacity for water absorption. The rising air velocities also resulted in the fall in temperature across this interface, successively leading to improved water retention as water evaporation has been reduced in the process. Fig. 6b displays the water content distribution for case A. In the presence of a cooling channel, a considerable increase in water content is relatively seen at the GDL-CL interface with increasing velocity of air. The range obtained for case A is between 1.9 and 2.3 in comparison with case B, which is

between 1.4 and 1.8. This improved water content in case A can be attributed to the improved cooling that reduces water evaporation caused by increased temperature.

channels a) without cooling

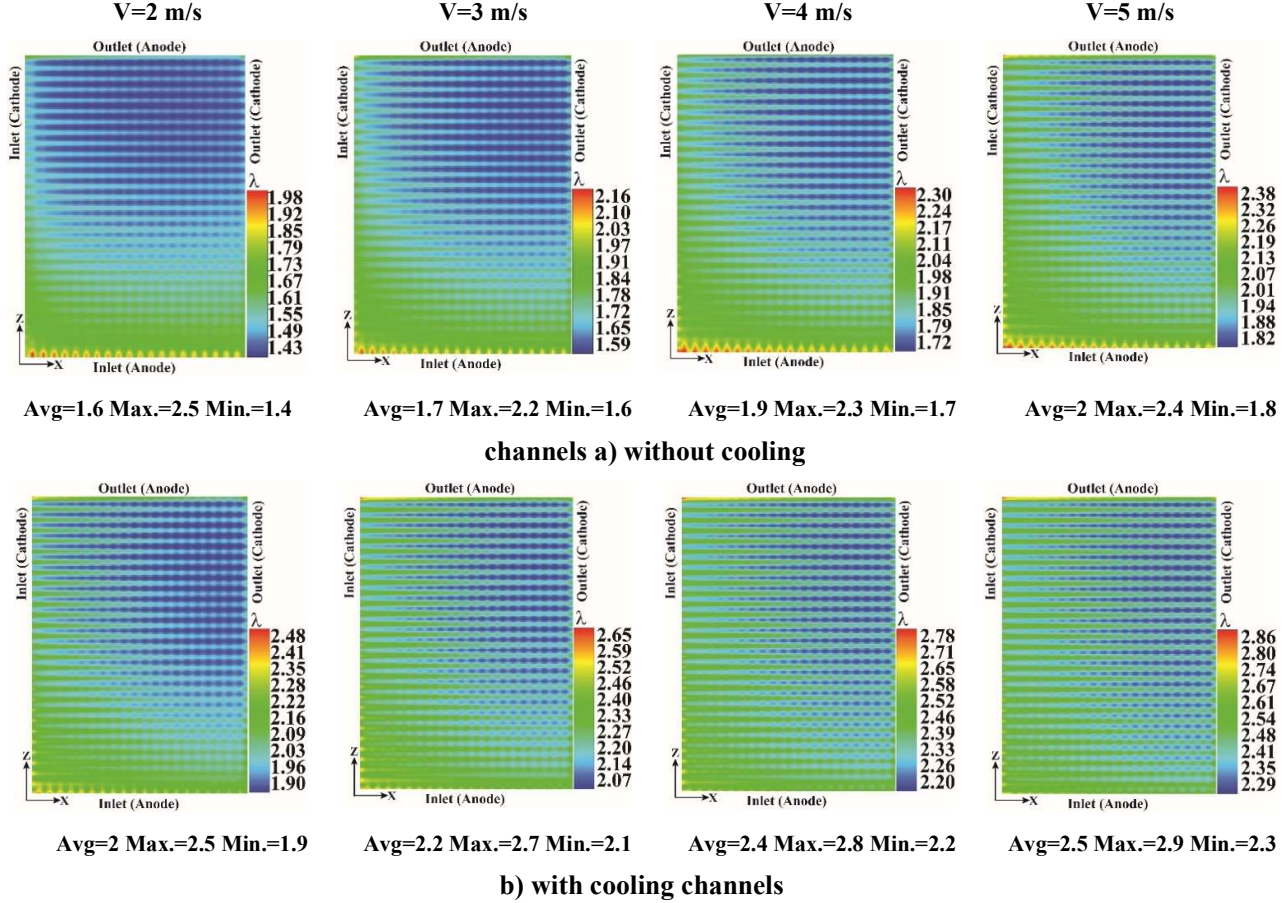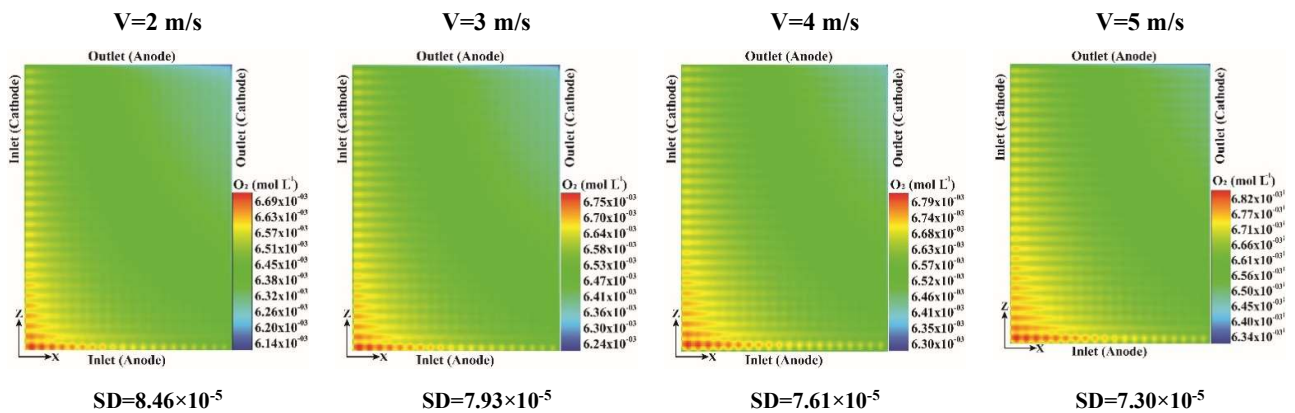**b) with cooling channels**

Fig. 6. Comparison of water content at GDL-CL interface

The distribution contours for the oxygen concentration in the CL-MEM interface are given in Fig. 7. The oxygen level near the cathode and anode inlets is visibly high in both cases but more apparent in case A. Low oxygen consumption at the inlet due to the high hydrogen concentrations at the anode inlet, electroosmotic drag raises water levels, resulting in water molecules being transported from the anode to the cathode. It decreases the consumption of oxygen during electrochemical reactions. It then limits cathode water absorption and therefore raises unconsumed oxygen concentration in this area. For cooling channels because of enhanced cooling and temperature reduction. Convective heat transport and water absorption are lower than in the rib region than in the channel and oxygen levels have dropped.

According to the figure, oxygen concentration on the catalyst surface increases with increasing air velocity without cooling channels. This is due to higher oxygen availability at the cathode catalyst layer. With cooling channels, oxygen concentration on the catalyst surface has increased with the increase in airflow rate; however, the increase in oxygen concentration is less than without cooling channels, which is undoubtedly due to the decrease in fuel cell temperature with airflow rate, which has an indirect effect on oxygen distribution.

According to the figure, oxygen concentration on the catalyst surface increases with increasing air velocity without cooling channels. This is due to higher oxygen availability at the cathode catalyst layer. With cooling channels, oxygen concentration on the catalyst surface has increased with an increase in air flow rate; however, the increase in oxygen concentration is less than without cooling channels, which is undoubtedly due to the decrease in fuel cell temperature with airflow rate, which has an indirect effect on oxygen distribution. Thus, it is very important to check the oxygen distribution on the catlayst layer. A smaller SD index indicates a more uniform distribution of oxygen. When the airflow rate in the cathode channels is equal to 2, 3, 4 and 5 m/s, SD for the fuel cell without cooling channels are 8.46×10^{-5}, 7.93×10^{-5}, 7.61×10^{-5}, and 7.30×10^{-5}, respectively. Changing the concentration of water in the polymer membrane fuel cell and the water content of the membrane is the opposite of changing the oxygen concentration. It means that when the oxygen concentration is low, the cathode side reactions occur at a higher rate, and more oxygen is consumed and less water is produced. It means that less oxygen is consumed when oxygen concentration is high, and more water is produced. This issue can be better understood by comparing Fig. 6 and Fig. 7. However, a more uniform distribution of oxygen also means a more uniform distribution of water. As a result, the uniformity index of the water content does not need to be calculated, and the change process of this index is the same for water content in two cases and at different air flow rates.
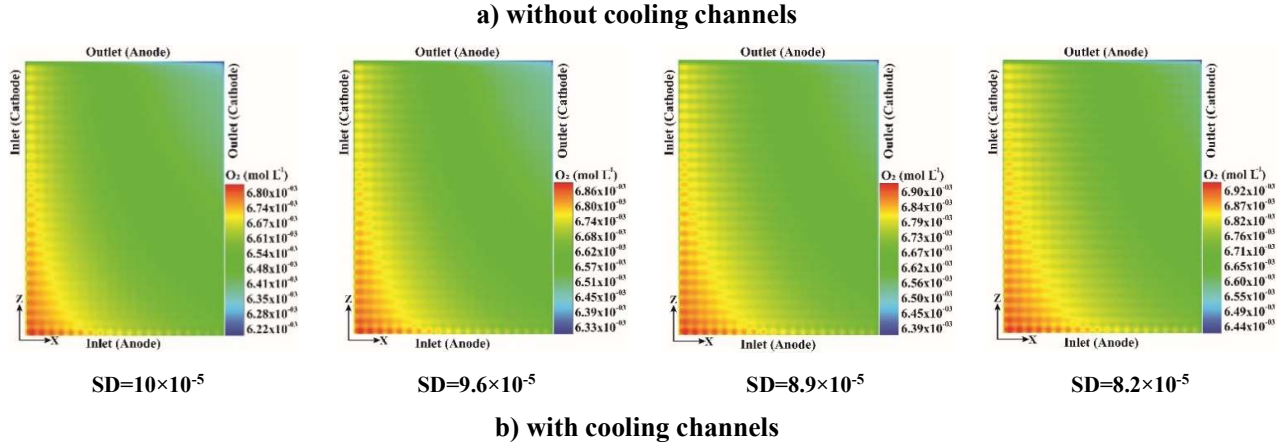
a) without cooling channels

| SD=10×10⁻⁵ | SD=9.6×10⁻⁵ | SD=8.9×10⁻⁵ | SD=8.2×10⁻⁵ |

b) with cooling channels

Fig. 7. Comparison of O$_2$ molar concentration at CL-MEM interface

3.3. Performance of the PEMFC systems

Fig. 8a provides the comparison of polarisation curves for the cases at different velocities. Behavior of the cell voltage considering activation, ohmic, and concentration losses are represented at various current densities. Activation loss is characterised by low electrochemical reaction in the catalyst region due to low activation overpotential. This overpotential is expected to increase with increasing temperature according to Butler-Volmer equation, thus reducing activation loss. The baseline case without cooling channels depicted better performance in the region of activation loss in contrast to case A due to the higher temperature caused by electrochemical reactions and reduced cooling activity, invariably leading to minor voltage loss. However, the current density and overall cell efficiency are more significant in case A's ohmic loss region than in case B. The loss in this region is due to the resistance to electron flow across the fuel cell components and is often propelled by high temperature. Thus, the high performance is seen in case A due to the relatively lower temperature observed in the interface of the components, as discussed previously. In the concentration loss region, the performance, especially in case A, decreases due to increased water production, resulting in a low oxygen supply at the CL. Moreover, increasing the velocity and minimizing temperature significantly reduced the current density. This means that at a velocity of 5 m/s, case A had the worst performance in terms of current density.

Electrical power densities for both cases are also illustrated in Fig. 8b. At 0.6 V voltage, the maximum and minimum output power was observed for case A at 5m/s, whereas the baseline case occurred at 2m/s. Generally, the installation of cooling channels increases the performance of the fuel cell in the ohmic zone as well as improves thermal performance but reduces the

performance of the fuel cell in the activation and concentration loss zones compared to the baseline case.
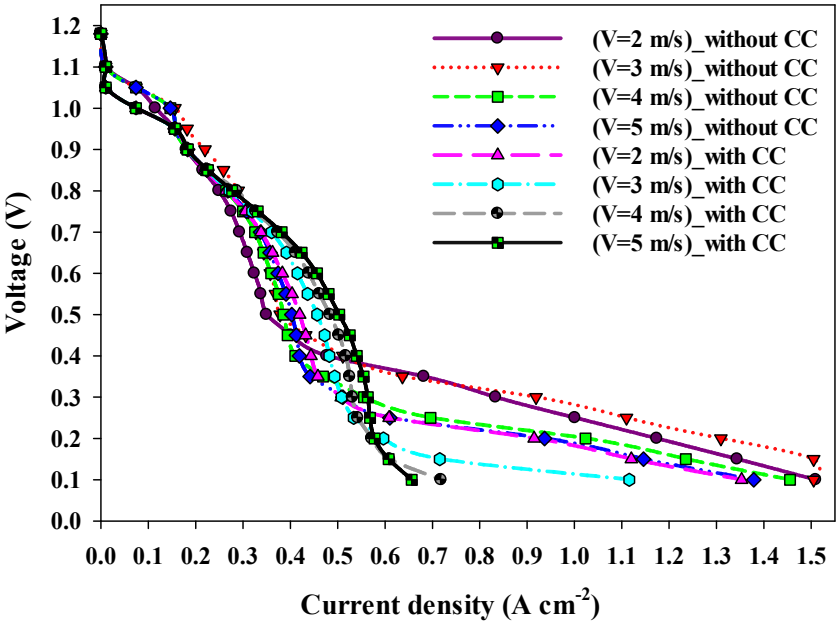
a)
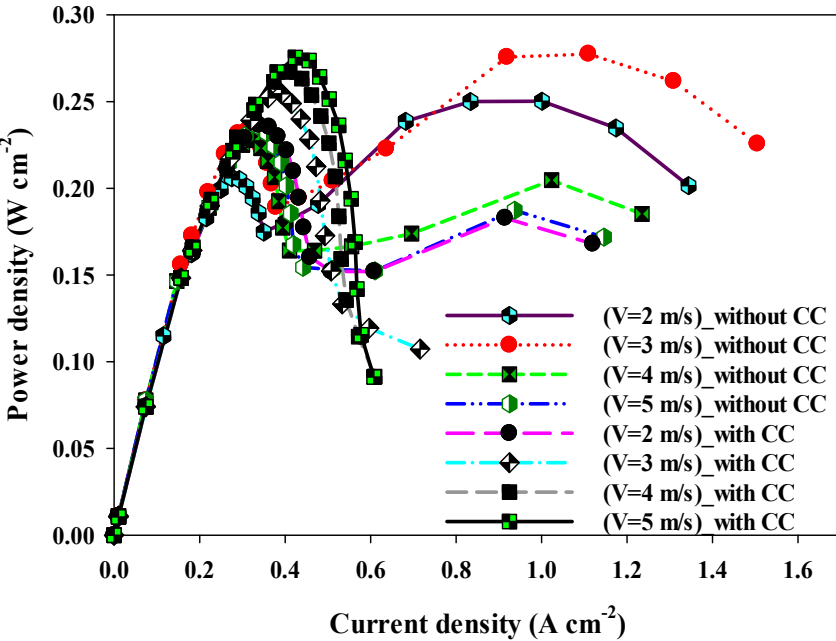
b)

Fig .8 a) Polarization curve; and b) Power density curve of case A and case B open-cathode PEMFC for varying air velocities [CC :cooling channel]

The net power outputs for the cases under study were also calculated considering the pressure drop across all the gas channels in both cases. In the open-cathode with external cooling channel – case A, the pressure drops in the cooling channels as well as the reactant gas channels were calculated. Typically, it will be ideal to consider the fan power input in calculating net power output. However, because the simulation was performed at similar air velocities, this effect was ignored and the losses due to individual pressure drops were investigated instead. The pressure drop observed in the cathode channel case A is significantly lower compared with the baseline case, as shown in Fig. 9. Unfavorable cooling causes more water absorption and reduces the gas mixture density in the lack of cooling channels, resulting in a higher average temperature. As a consequence, there was a little gain in velocity and a slight decrease in pressure drop.

It should be noted that, although better thermal performance is evident in case A, its total pressure drop is higher than that of the baseline case.

At an air velocity of 5m/s, case A and case B produced 28 and 22 watts of electrical power, while the parasitic power due to pressure drops was calculated to be 0.34 and 0.03 watts, respectively. The net power output calculated from the difference between the measured power and parasitic power is 27.66 and 21.97 watts for case A and case B, respectively. Ultimately, case A produces high power output compared with the case without cooling channels.
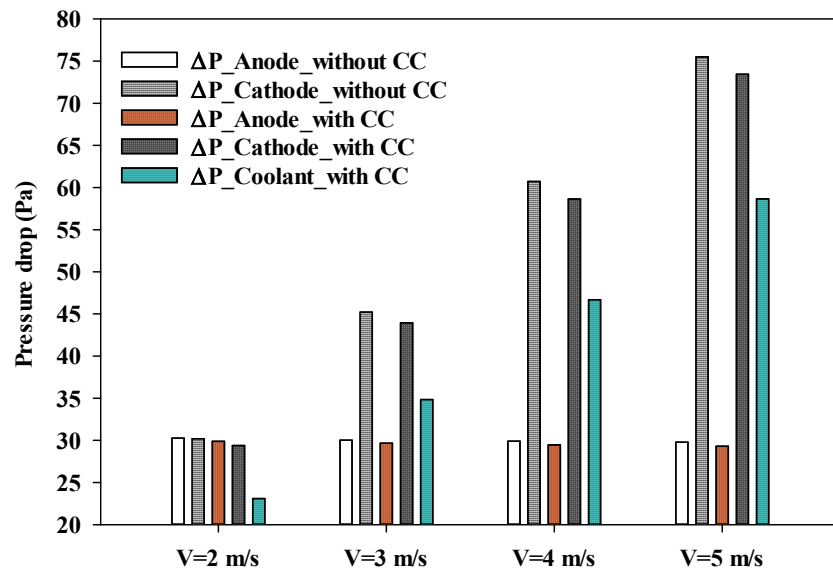

Fig. 9. Comparison of pressure drop

Conclusion

A three-dimensional multiphase model, accounting for contact resistance at the GDL/BPP interface was developed to assess the performance of an open-cathode PEM fuel cell with external cooling channels. This was benchmarked against the conventional forced open-cathode PEMFC under similar operating conditions. The following can be concluded from this research:

1. The presence of an additional cooling channel, as in case A, improves the cooling capability of the fuel cell. Moreso, the cell temperature is reduced, consequently mitigating water retention and stabilizing proton transfer across the membrane. Thus, improving fuel cell performance.

2. Increasing the airflow rate improves cooling and enhances the thermal performance of the fuel cells.

3. As observed in the activation loss zone, lowering the cell temperature by increasing the airflow rate or adding a separate cooling channel has a negative impact on the cell's performance. Conversely, in the ohmic region, due to the cell's favorable condition of maintaining the membrane's water content and reducing the ohmic resistance, increasing airflow speed in case A improves cell performance and power output. In the concentration loss zone of the polarization curve, the case with the cooling channel has a reduced performance due to a large volume of water production, which reduces oxygen access to the catalyst layer, thus decreasing the density of the electric current produced.

4. The difference in output power at the maximum voltage of 0.65 cell power reached 6.3 watts. However, the parasitic consumption due to pressure drop in the case with and without cooling channels for each cell is 0.34 and 0.03, respectively.

To sum up, the case with the cooling channel had a better performance but imposed enormous parasitic power due to high-pressure drop on the fuel cell, which reduced the net power output. A techno-economic assessment of the fuel cells will improve determining the cost-benefit tradeoff between performance and cost of the additional cooling channel.

Nomenclature

A	Area, $[m^2]$
BPP	Bipolar Plate
CL	Catalyst layer
EW	Equivalent weight of a dry membrane, $[kg\ mol^{-1}]$
GDL	Gas diffusion layer
HOR	Hydrogen oxidation reaction
MEA	Membrane electrode assembly
MF	Metal foam
ORR	Oxygen reduction reaction
a_r	Ratio of an electrochemically active area of CL to CL volume, $[m^{-1}]$
a	Water activity
C_{H_2}/C_{O_2}	Molar concentration of H_2/O_2, $[mol\ m^{-3}]$
$C_{H_2,ref}/C_{O_2,ref}$	Reference molar concentration of H_2/O_2, $[mol\ m^{-3}]$
C_p	Specific heat at constant pressure, $[J\ kg^{-1}K^{-1}]$
c_r	Water condensation rate constant
D_i	Species diffusivity, $[m^2\ s^{-1}]$
D_i^0	Reference Species diffusivity, $[m^2\ s^{-1}]$
d_p	Mean particle diameter, $[m]$
E_0	Open circuit voltage, $[V]$
F	Faraday's constant, 96,487 $[C\ mol^{-1}]$
h_{fg}	Latent heat of vapor-water phase change, $[kJ\ kg^{-1}]$
i_0	Exchange current density, $[A\ m^{-2}]$
I	Applied current density, $[A\ cm^{-2}]$
k	Thermal conductivity, $[W\ m^{-1}K^{-1}]$
K_p	Permeability, $[m^2]$
M_w	Molecular weight, $[kg\ mol^{-1}]$
n	Number of electrons transferred in the electrode reaction
n_d	Electroosmotic drag coefficient
P	Pressure, $[Pa]$
P_c	Capillary pressure, $[Pa]$
R	Universal gas constant, 8.314 $[J\ mol^{-1}K^{-1}]$
$R_{GDL/BPP}$	Electric contact resistance, $[s^{-1}\ m]$
j	Transfer current density, $[A\ m^{-3}]$
r_s	Saturation exponent
S	Source term
s	Liquid saturation
T	Temperature, $[K]$
$\vec{u}$	Fluid velocity and superficial velocity in a porous medium, $[m\ s^{-1}]$
W	Power density, $[W\ cm^{-2}]$

Greek

α	Transfer coefficient
ε	Porosity
η	Surface overpotential, $[V]$
λ	Water content
μ	Dynamic viscosity, $[kg\ s\ m^{-2}]$
ρ	Density, $[kg\ m^{-3}]$
σ	Electrical conductivity, $[S\ m^{-1}]$
σ_{surf}	Surface tension, $[N\ m^{-2}]$
ξ	Stoichiometric flow ratio
γ	Reaction order

φ	Phase potential, [V]
τ	Viscous shear stress, [N m^{-2}]
κ	Proton conductivity, [S m^{-1}]
θ_c	Contact angle (°)

Superscripts

g	Gas phase
eff	Effective coefficient
l	Liquid phase
mem	Membrane
ref	Reference
0	Reference

Subscripts

Assembly	Assembly of cells
a	Anode
c	Cathode
comp	Compress
contact	GDL and BP interface area, [m^2]
l	Liquid
mem	Membrane
u	Momentum source term subscript
ref	Reference
s	Solid phase
surf	surface tension
sat	Saturation
sol	Solid
w	Water
wv	Water vapor

References

[1]   Atyabi SA, Afshari E. Three-dimensional multiphase model of proton exchange membrane fuel cell with honeycomb flow field at the cathode side. J Clean Prod 2019;214:738–48. doi:10.1016/j.jclepro.2018.12.293.

[2]   Wang Y, Ruiz Diaz DF, Chen KS, Wang Z, Adroher XC. Materials, technological status, and fundamentals of PEM fuel cells – A review. Mater Today 2020;32:178–203. doi:10.1016/j.mattod.2019.06.005.

[3]   Atyabi SA, Afshari E. A numerical multiphase CFD simulation for PEMFC with parallel sinusoidal flow fields. J Therm Anal Calorim n.d. doi:10.1007/s10973-018-7270-3.

[4]   Toghyani S, Atyabi SA, Gao X. Enhancing the Specific Power of a PEM Fuel Cell Powered UAV with a Novel Bean - Shaped Flow Field. Energies 2021;14:2494.

[5]   Kurnia JC, Chaedir BA, Sasmito AP, Shamim T. Progress on open cathode proton exchange membrane fuel cell: Performance, designs, challenges and future directions. Appl Energy 2021;283:116359.

[6]   Sasmito AP, Lum KW, Birgersson E, Mujumdar AS. Computational study of forced air-

convection in open-cathode polymer electrolyte fuel cell stacks. J Power Sources 2010;195:5550–63. doi:10.1016/j.jpowsour.2010.02.083.

[7]   Saufi Sulaiman M, Singh B, Mohamed WANW. Experimental and theoretical study of thermoelectric generator waste heat recovery model for an ultra-low temperature PEM fuel cell powered vehicle. Energy 2019;179:628–46. doi:10.1016/j.energy.2019.05.022.

[8]   Atyabi SA, Afshari E, Zohravi E, Udemu CM. Three-dimensional simulation of different flow fields of proton exchange membrane fuel cell using a multi-phase coupled model with cooling channel. Energy 2021;234:121247. doi:10.1016/j.energy.2021.121247.

[9]   López-Sabirón AM, Barroso J, Roda V, Barranco J, Lozano A, Barreras F. Design and development of the cooling system of a 2 kW nominal power open-cathode polymer electrolyte fuel cell stack. Int J Hydrogen Energy 2012;37:7289–98. doi:10.1016/j.ijhydene.2011.11.073.

[10]   Liu JX, Guo H, Ye F, Ma CF. Two-dimensional analytical model of a proton exchange membrane fuel cell. Energy 2017;119:299–308.

[11]   Afshari E, Mosharaf-Dehkordi M, Rajabian H. An investigation of the PEM fuel cells performance with partially restricted cathode flow channels and metal foam as a flow distributor. Energy 2017;118:705–15. doi:10.1016/j.energy.2016.10.101.

[12]   Abdollahzadeh M, Pascoa JC, Ranjbar AA, Esmaili Q. Analysis of PEM (Polymer Electrolyte Membrane) fuel cell cathode two-dimensional modeling. Energy 2014;68:478–94. doi:10.1016/j.energy.2014.01.075.

[13]   Rahgoshay SM, Ranjbar AA, Ramiar A, Alizadeh E. Thermal investigation of a PEM fuel cell with cooling flow field. Energy 2017;134:61–73. doi:10.1016/j.energy.2017.05.151.

[14]   Pan M, Li C, Liao J, Lei H, Pan C, Meng X, et al. Design and modeling of PEM fuel cell based on different flow fields. Energy 2020;207. doi:10.1016/j.energy.2020.118331.

[15]   Cai Y, Fang Z, Chen B, Yang T, Tu Z. Numerical study on a novel 3D cathode flow field and evaluation criteria for the PEM fuel cell design. Energy 2018;161:28–37. doi:10.1016/j.energy.2018.07.127.

[16]   Karst N, Faucheux V, Martinent A, Bouillon P, Laurent JY, Druart F, et al. Innovative water management in micro air-breathing polymer electrolyte membrane fuel cells. J Power Sources 2010;195:1156–62. doi:10.1016/j.jpowsour.2009.08.068.

[17]   Matian M, Marquis A, Brandon N. Model based design and test of cooling plates for an

air-cooled polymer electrolyte fuel cell stack. Int J Hydrogen Energy 2011;36:6051–66. doi:10.1016/j.ijhydene.2011.01.026.

[18]   Qiu D, Peng L, Tang J, Lai X. Numerical analysis of air-cooled proton exchange membrane fuel cells with various cathode flow channels. Energy 2020;198:117334. doi:10.1016/j.energy.2020.117334.

[19]   Zhao J, Huang Z, Jian B, Bai X, Jian Q. Thermal performance enhancement of air-cooled proton exchange membrane fuel cells by vapor chambers. Energy Convers Manag 2020;213:112830. doi:10.1016/j.enconman.2020.112830.

[20]   Kang DG, Park C, Lim IS, Choi SH, Lee DK, Kim MS. Performance enhancement of air-cooled open cathode polymer electrolyte membrane fuel cell with inserting metal foam in the cathode side. Int J Hydrogen Energy 2020;45:27622–31. doi:10.1016/j.ijhydene.2020.07.102.

[21]   Sagar A, Chugh S, Sonkar K, Sharma A, Kjeang E. A computational analysis on the operational behaviour of open-cathode polymer electrolyte membrane fuel cells. Int J Hydrogen Energy 2020;45:34125–38. doi:10.1016/j.ijhydene.2020.09.133.

[22]   Huang Z, Jian Q, Zhao J. Thermal management of open-cathode proton exchange membrane fuel cell stack with thin vapor chambers. J Power Sources 2021;485:229314. doi:10.1016/j.jpowsour.2020.229314.

[23]   Lee N, Salihi H, Yoo B, Lee J, Lee SW, Jang SS, et al. Metal-foam-based cathode flow-field design to improve H2O retention capability of passive air cooled polymer electrolyte fuel cells. Int J Therm Sci 2021;161:106702. doi:10.1016/j.ijthermalsci.2020.106702.

[24]   Lee J, Gundu MH, Lee N, Lim K, Lee SW, Jang SS, et al. Innovative cathode flow-field design for passive air-cooled polymer electrolyte membrane (PEM) fuel cell stacks. Int J Hydrogen Energy 2020;45:11704–13. doi:10.1016/j.ijhydene.2019.07.128.

[25]   Hu M, Gu A, Wang M, Zhu X, Yu L. Three dimensional, two phase flow mathematical model for PEM fuel cell: Part I. Model development. Energy Convers Manag 2004;45:1861–82. doi:10.1016/j.enconman.2003.09.022.

[26]   Sukkee Um C -Y. W, Chen KS. Computational Fluid Dynamics Modeling of Proton Exchange Membrane Fuel Cells. J Power Sources 2000;147:95–106. doi:10.1016/j.jpowsour.2005.01.011.

[27]   Zhao C, Xing S, Liu W, Wang H. Air and H2 feed systems optimization for open-cathode proton exchange membrane fuel cells. Int J Hydrogen Energy 2021;46:11940–51. doi:10.1016/j.ijhydene.2021.01.044.

[28] Lee J, Salihi H, Lee J, Ju H. Impedance modeling for polymer electrolyte membrane fuel cells by combining the transient two-phase fuel cell and equivalent electric circuit models. Energy 2022;239:122294. doi:10.1016/j.energy.2021.122294.

[29] Mazumder S, Cole JV. Rigorous 3-D Mathematical Modeling of PEM Fuel Cells. J Electrochem Soc 2003;150:A1510. doi:10.1149/1.1615609.

[30] Shahsavari S, Desouza A, Bahrami M, Kjeang E. Thermal analysis of air-cooled PEM fuel cells. Int J Hydrogen Energy 2012;37:18261–71. doi:10.1016/j.ijhydene.2012.09.075.

[31] Bradley TH, Moffitt BA, Mavris DN, Parekh DE. Development and experimental characterization of a fuel cell powered aircraft. J Power Sources 2007;171:793–801. doi:10.1016/j.jpowsour.2007.06.215.